Journal of ELECTRONIC MATERIALS, Vol. 49, No. 2, 2020
https://doi.org/10.1007/s11664-019-07825-z

Comprehensive Study of Structural, Magnetic and Dielectric Properties of Borate/Fe_3O_4 Glass Nanocomposites

T.A. TAHA,[1,2,5] A.A. AZAB,[3] and E.H. EL-KHAWAS[4]

1.—Physics Department, College of Science and Arts, Jouf University, P.O. Box 756, Al-Gurayyat, Saudi Arabia. 2.—Physics and Engineering Mathematics Department, Faculty of Electronic Engineering, Menoufia University, Menouf 32952, Egypt. 3.—Solid State Electronics Laboratory, Physics Division, Solid State Physics Department, National Research Centre, 33 El Bohouth St., Dokki, Giza 12622, Egypt. 4.—Basic Science Department, Higher Technological Institute, Tenth of Ramadan City, Egypt. 5.—e-mail: taha.hemida@yahoo.com

The objective of this work is to study the structural, magnetic and dielectric properties of 60 B_2O_3-10 ZnO-30-NaF: x Fe_3O_4 (x = 0.0 wt.%, 3.0 wt.%, 6.0 wt.%, 9.0 wt.%, 12 wt.% and 20 wt.%) glass nanocomposites. X-ray diffraction measurements indicated that the samples were amorphous except for the glass sample containing 20.0 wt.% Fe_3O_4, revealing the presence of a nanocrystalline magnetite phase having a cubic crystal structure with an average size of 24.10 ± 1.79 nm. Transmission electron microscopy analysis showed that Fe_3O_4 nanoparticles with an average size of 24.0 nm were dispersed homogeneously inside the borate glass matrix. Fourier transform infrared spectra of these samples exhibited bands from 422 cm^{-1} to 492 cm^{-1} for the vibration of the Fe-O bond in the [FeO_4] group and vibration modes of BO_3 and BO_4 units. Magnetic analysis of these glasses revealed paramagnetic-like behaviors, with a very narrow hysteresis loop and very low coercivity (H_c), close to those of typical soft magnetic materials. The relative permittivity was increased and the dielectric loss ε'' was enhanced with increasing Fe_3O_4 concentration. The energy needed to move the electron from one location to infinity (W_M) increased from 0.18 to 1.28 eV with an increase in Fe_3O_4 content. Finally, the AC conductivity was enhanced with the addition of magnetite.

Key words: Glass nanocomposite, Fe_3O_4, magnetic properties, dielectric constant

INTRODUCTION

Research into the preparation of oxide glasses containing iron oxide compounds has garnered considerable attention in recent years.[1–3] Each application requires magnetic nanoparticles with different properties. For example, in data storage applications, the particles need to have a stable, switchable magnetic state to represent bits of information, a state that is not affected by temperature fluctuations. In the case of biomedical applications, particles with superparamagnetic behavior at room temperature (no remanence along with a rapidly changing magnetic state) are chosen.[4]

Preparation methods involving micelles, co-precipitation and dispersion in matrices such as silica, alumina and polymers are attracting increasing research attention, as they provide both a controllable and narrow distribution of particle size and morphology.[5–10] Among these, nanostructured materials prepared via a glass route possess advantages over others because of the easier preparation and cost-effectiveness, and the ability to control the crystal nucleation and growth processes enables fine-grained microstructures to be achieved.[11–15] Moreover, some bioactive magnetic glass ceramics can be fabricated (can bind to natural tissues via a

(Received September 3, 2019; accepted November 9, 2019; published online November 21, 2019)

hydroxyapatite layer) and can be used to fill bone defects resulting from tumor surgery.[16]

In this work, the fabrication and structural and magnetic properties of borate/Fe_3O_4 magnetic nanoglass composites are considered. The as-prepared glassy samples were not subjected to further heat treatment, and no nucleating agents were used in their crystallization process, due to the high crystal nucleation rates. The effect of Fe_3O_4 incorporated in the borate glass matrix on the magnetic and dielectric characteristics of glass nanocomposite samples is also analyzed.

EXPERIMENTAL

Our nontraditional glass matrix composites were prepared by melting raw material (mixed from B_2O_3, ZnO, NaF and Fe_3O_4 according to the formula 60 B_2O_3-10 ZnO-30-NaF: $x$$Fe_3O_4$ (x = 0.0 wt.%, 3.0 wt.%, 6.0 wt.%, 9.0 wt.% and 20 wt.%). After melt temperature equilibration (~1150°C) for 30 min and rapid quenching between two stainless steel plates, a solid specimen (about 1.5 mm thick) was formed.

The x-ray diffraction (XRD) examination of the glass system was performed utilizing a D8 Advance system (Bruker AXS GmbH, Germany), with CuKα-radiation ($\lambda_{k\alpha}$ = 1.542 Å). Transmission electron microscopy (TEM) micrographs of the glass nanocomposite were collected via a JEOL JEM-200CX transmission electron microscope (Japan). Fourier transform infrared (FTIR) spectroscopy of the glass composites was completed within the range 400–4000 cm^{-1} via a JASCO FT/IR-6100 spectrometer (Japan). A vibrating-sample magnetometer (7410 Series VSM; Lake Shore Cryotronics, Westerville, OH, USA) was used to measure the magnetic properties of the glass nanocomposites. Dielectric data were collected at 300 K using broadband dielectric spectroscopy (Alpha High-Resolution Analyzer (Novocontrol GmbH) assisted by Quatro temperature controls with high temperature stability) across a wide range of frequencies.

RESULTS AND DISCUSSION

As shown in Fig. 1, the XRD spectra of the as-made glass composites revealed the amorphous nature of the glass samples containing 0.0 wt.%, 3.0 wt.%, 6.0 wt.%, 9.0 wt.% and 12.0 wt.% Fe_3O_4, while the sample containing 20.0 wt.% showed the presence of a nanocrystalline magnetite phase having a cubic crystal structure (compared with JCPDS Card No. 88-0315).

Easy particle crystallization in the (222) direction of Fe_3O_4 results in peak intensity (222) comparatively higher than other peaks. From the obtained peak of the XRD pattern, the crystal size of Fe_3O_4 was estimated via the Williamson-Hall method to be 24.10 ± 1.79 nm, according to different positions and separation of size and strain broadening analysis[7] utilizing XPowder software.

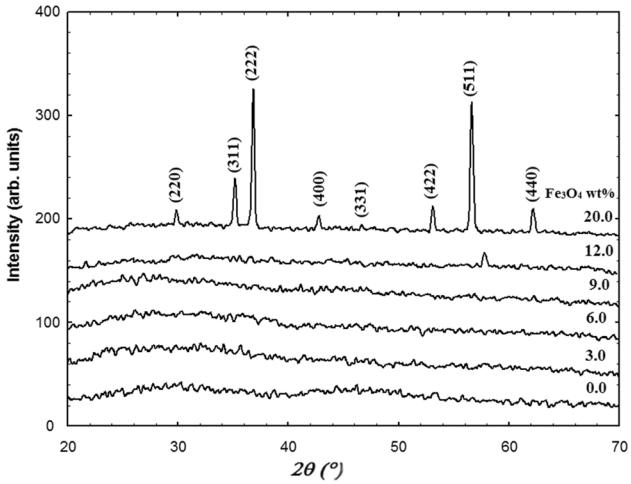

Fig. 1. XRD spectra of the prepared borate glass samples containing Fe_3O_4.

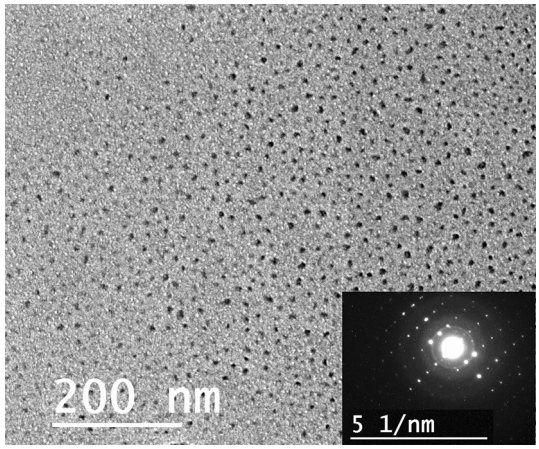

Fig. 2. TEM measurements of the borate glass matrix containing 20.0 wt.% Fe_3O_4.

TEM micrograph measurements for the glass sample containing 20 wt.% Fe_3O_4 are depicted in Fig. 2. It is obvious that the Fe_3O_4 nanoparticles were grown inside the borate glass matrix homogeneously, with particle size around 24.0 nm, which is consistent with XRD estimation.

Examination of Fourier transform infrared (FTIR) spectra of the as-prepared glass samples as shown in Fig. 3 evidenced broad reflection bands because of the wide distribution of the structural units, given in Table I.

In all the measured FTIR spectra, the bands from 422 cm^{-1} to 492 cm^{-1} are caused by the vibration of the Fe-O bond in the [FeO_4] group, and the peaks from 547 cm^{-1} to 644 cm^{-1} represent B-O-B bending vibration.[17,18] The stretching vibration of the B-O bond and symmetric stretching vibration of the O-B-O bond in the [BO_4] group are located at (808 cm^{-1}–867 cm^{-1}) and (1027 cm^{-1}–1031 cm^{-1}).[19–21]

The bands from 1118 cm^{-1} to 1197 cm^{-1} correspond to B-O stretch in BO_4 units from tri-, tetra- and pentaborate groups; however, that from 1263 cm^{-1} to 1270 cm^{-1} represents B-O symmetric stretching in BO_3 units from pyro- and ortho-borate groups.[22] The peak around 1390 cm^{-1} is attributed to asymmetric stretching of B-O of trigonal BO_3.[23] The bands at (1423–1450 cm^{-1}) and (~1630 cm^{-1}) are ascribed to B-O- stretch in BO_2O- units from different borate groups and asymmetric stretching relaxation of the B-O band of the trigonal BO_3 units.[22] Additionally, vibrational bands due to hydrogen bonding and molecular water appear in the infrared range 2856–3446 cm^{-1}.[24]

The magnetization hysteresis loops for the composite glass-magnetite with different Fe_3O_4 content are depicted in Fig. 4. The samples showed paramagnetic-like behavior with no saturation and very narrow hysteresis loop (very low values of both coercivity (H_c) and remanence magnetization). This paramagnetic-like behavior for the composite glass-magnetite originated from the amorphous glass structure which causes the orientation of the magnetic dipole of magnetite to be randomly distributed. If the magnetite clusters occupy the pores in the glass, the interaction between magnetite ions is weak.[25,26]

Figure 5 shows the related magnetic parameters (saturation magnetization M_S, coercivity H_C, remanence M_r) taken from M-H loops shown in Fig. 4 and listed in Table II. The saturation magnetization M_S increases with an increase in magnetite content due to the increase in ferromagnetic magnetic content. The remanence magnetization (M_r) and coercivity H_C exhibit the same behavior with magnetite concentration, where they increase with

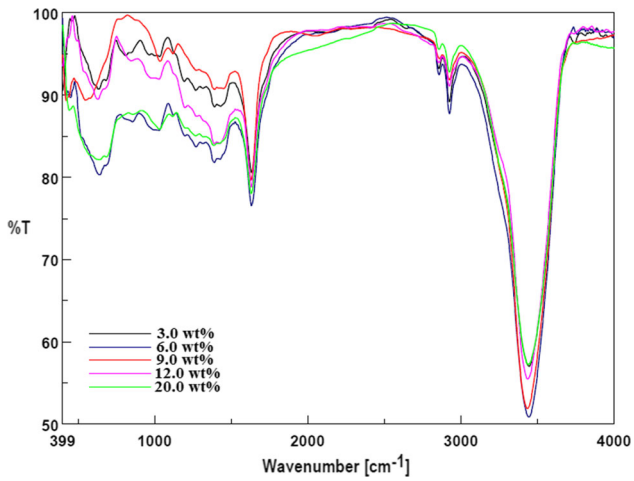

Fig. 3. FTIR spectra of the as-prepared glass samples.

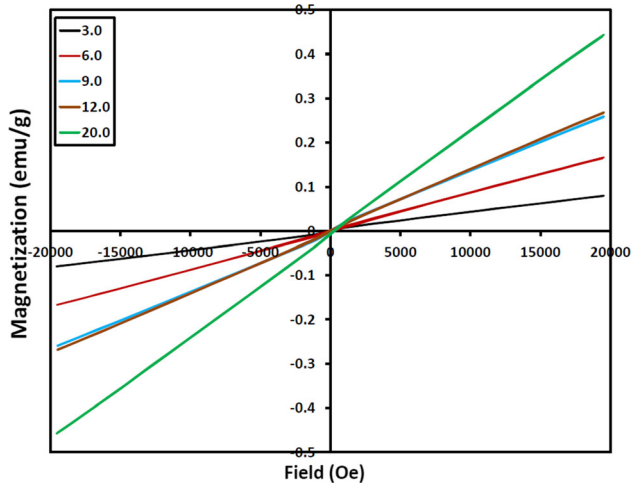

Fig. 4. VSM hysteresis loops of borate/Fe_3O_4 glass nanocomposites.

Table I. The absorption band positions obtained from FTIR spectra

Sample	3.0	6.0	9.0	12.0	20.0	Assignment
A	457	451	422	492	441	Vibration of Fe-O bond in [FeO_4] group
B	630	644	547	628	634	Bending vibration of B-O-B bonds
C	808	854	867	846	860	Stretching vibration of B-O bond in [BO_4] group
D	1031	1027	1035	1028	1031	Symmetric stretching vibration of O-B-O bond in [BO_4] group
E	1193	1122	1118	1197	1118	B-O stretch in BO_4 units from tri-, tetra- and pentaborate groups
F	1268	1270	1263	1263	1267	B-O symmetric stretching in BO_3 units from pyro- and ortho-borate groups
G	1390	1390	1390	1390	1388	Asymmetric stretching of B-O of trigonal BO_3
H	1430	1423	1450	1427	1448	B-O- stretch in BO_2O- units from different borate groups
I	1630	1631	1629	1631	1631	Asymmetric stretching relaxation of the B-O band of trigonal BO_3 units
J	2856, 2925	2858, 2925	2860, 3925	2856, 2925	2858, 2925	Hydrogen bonding
K	3446	3444	3443	3436	3440	Water

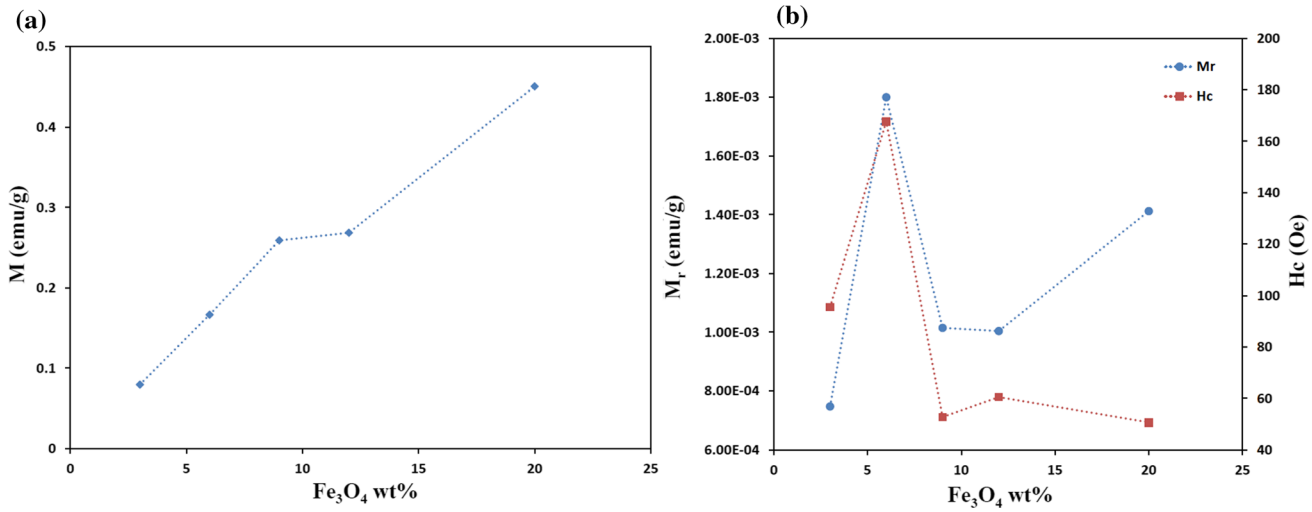

Fig. 5. (a) The saturation magnetization M_S, (b) coercivity H_C and remanence M_r versus Fe_3O_4 concentration.

Table II. Magnetic parameters of borate/Fe_3O_4 glass nanocomposites

Sample	M_s (emu/g)	H_c (Oe)	M_r (emu/g)	R_s	W_M (eV)
3.0	0.08	59.13	0.00075	0.0094	0.18
6.0	0.17	176.67	0.0018	0.0011	0.22
9.0	0.26	35.71	0.0010	0.0039	0.20
12.0	0.27	62.11	0.0010	0.0037	0.21
20.0	0.45	50.62	0.0014	0.0031	1.28

magnetite content, but they have a sharp maximum value at Fe_3O_4 = 6.0 wt.%. Remanence magnetization refers to the magnetization left behind in a ferromagnetic material after an external magnetic field is removed (residual magnetization). The remanence of magnetic materials provides the magnetic memory in magnetic devices.

The remanence magnetization and coercivity are affected by the crystal shape and size, residual stress and crystal imperfections.[27] The variation in the remanence magnetization and coercivity with Fe_3O_4 content may be due to the structural atomic distribution of iron ions in the vitreous matrix.[28] The magnetic properties of nanoparticles depend on intrinsic magnetocrystalline anisotropy, shape anisotropy and particle size. However, the shape anisotropy is the dominant form of anisotropy, being more important than magnetocrystalline anisotropy. The behavior of Hc in the composite may be due to changes in particle size and shape anisotropy, where coercivity increases with increasing particle size when the particle size is smaller than single-domain size.[29] The squareness ratio is computed from the equation $R_s = \frac{M_r}{M_s}$[7] and R_s values listed in Table II; their values generally increase with Fe_3O_4 content and depict properties of soft magnetism.

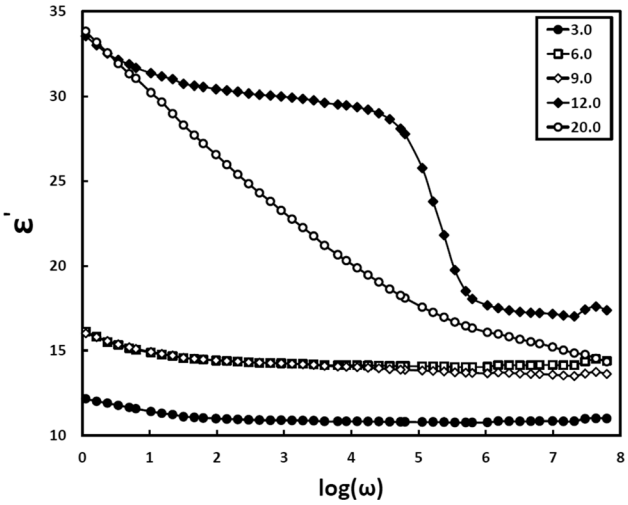

Fig. 6. The frequency-dependent dielectric constants of the glass/nanocomposite samples.

The complex dielectric permittivity (ε^*) is a very important parameter obtained from dielectric relaxation spectroscopy which is given by Eq. 1[30,31]:

$$\varepsilon^* = \varepsilon' - i\varepsilon'' \quad (1)$$

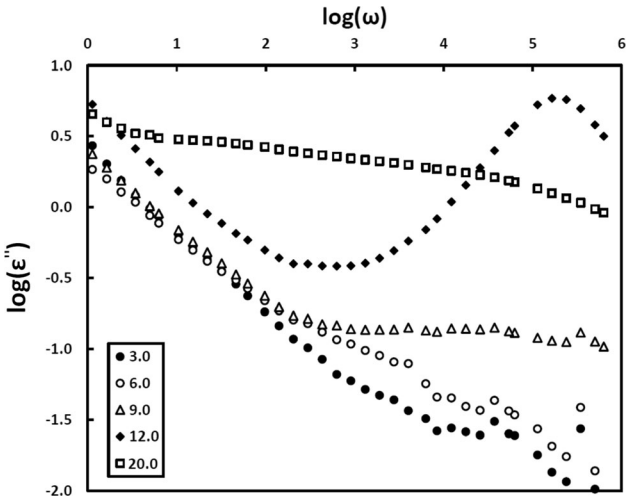

Fig. 7. The frequency-dependent dielectric loss of the glass/nanocomposites.

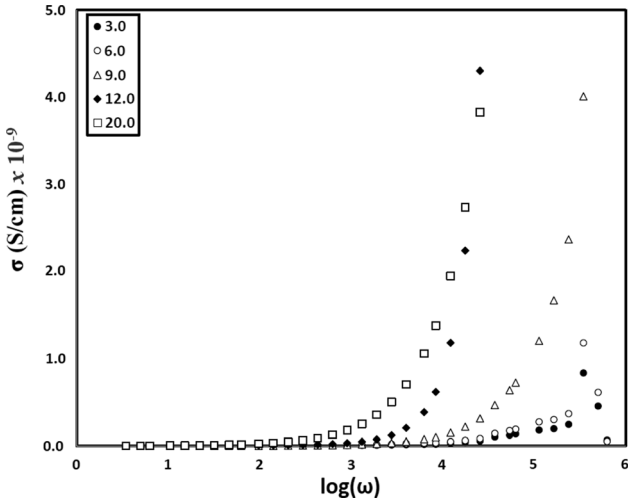

Fig. 8. AC conductivity versus frequency for borate/Fe_3O_4 nanocomposites at 300 K.

Relative permittivity ε', (the real part) in this case, measures the material's capacity for polarization and storing electrical loads when it is used in condensers. The dielectric loss ε'' (imaginary part) comes from dipole formation and alignment. Figure 6 shows that relative permittivity decreases with an increase in frequency, likely due to mobile ion polarization, while ε' increases with increased Fe_3O_4 concentration due to conduction and polarization coupling into a single process.[32]

The variation in dielectric loss $\log(\varepsilon'')$ of the glass nanocomposites with frequency is shown in Fig. 7. It is clearly seen that at low frequency, ε'' decreases with frequency. The dielectric loss of the borate glass matrix is enhanced with the gradual addition of Fe_3O_4. The function specifies that the frequency dependence of ε'' within the moderate range is[33,34]:

$$\varepsilon'(\omega) = (\varepsilon_s - \varepsilon_\infty)2\pi^2 N\left(ne^2/\varepsilon_s\right)^3 k_\beta T\tau_0^m W_M^{-4}\omega^{-m} \quad (2)$$

where $m = -4\,k_\beta\,T/W_M$, N is the localized states concentration, n equals the number of electrons, and W_M is the energy needed to shift the electron from one position to infinity. The values of W_M (recorded in Table II) were estimated and are found to increase from 0.18 eV to 1.28 eV with increasing Fe_3O_4 content.

The impact of frequency on AC conductivity (σ) at 300 K for the glass nanocomposites is displayed in Fig. 8; the AC conductivity increases with frequency for all nanocomposites due to the high energy applied on the charge carrier, increasing the charge carrier hopping or tunneling. Also, the AC conductivity is enhanced with the addition of magnetite to the borate glass matrix, which is ascribed to the continual formation of conductive pathways in the glass network and a relative tendency of charge carrier hopping or increase in the number of glass network defects.[32]

CONCLUSION

Borate/Fe_3O_4 magnetic nano-glass composites were prepared via a quenching route without further thermal treatment. XRD study showed the presence of a nanocrystalline magnetite with particle size 24.10 ± 1.79 nm, and TEM measurements confirmed the formation of Fe_3O_4 with particle size of around 24.0 nm. FTIR reflection spectra indicated Fe-O, B-O-B, O-B-O and B-O vibration bands. VSM analysis revealed paramagnetic-like behavior of the composite glass-magnetite, and the saturation magnetization M_S increased with an increase in magnetite content due to the increase in ferromagnetic magnetic content. The relative permittivity ε' and dielectric loss ε'' were enhanced with an increase in Fe_3O_4 concentration, and the W_M values were increased from 0.18 eV to 1.28 eV with an increase in Fe_3O_4 content. Finally, the AC conductivity was enhanced with the addition of magnetite to the borate glass matrix, which is ascribed to the continual formation of conductive pathways in the glass network.

CONFLICT OF INTEREST

The corresponding author states that there is no conflict of interest.

REFERENCES

1. L. Rus, S. Rada, V. Rednic, E. Culea, M. Rada, A. Bot, N. Aldea, and T. Rusu, *J. Non Cryst. Solids* 402, 111 (2014).
2. M. Georgieva, D. Tzankov, R. Harizanova, G. Avdeev, and C. Russel, *Appl. Phys. A Mater. Sci. Process.* 122, 160 (2016).
3. A.A. Osipov, R.T. Zainullina, L.M. Osipova, M.V. Shtenberg, P.V. Khvorov, and S.M. Lebedeva, *Glass Phys. Chem.* 44, 211 (2018).
4. P. Tartaj, M.P. Morales, S. Veintemillas-Verdaguer, T. Gonzalez-Carreno, and C.J. Serna, *J. Phys. D Appl. Phys.* 36, R182 (2003).
5. M.M. Rashad, D.A. Rayan, M. El-Gendy, M.M. El Kholy, and T.A. Taha, *J. Supercond. Nov. Magn.* 31, 4191 (2018).
6. T.A. Taha, S. Elrabaie, and M.T. Attia, *J. Mater. Sci.: Mater. Electron.* 29, 18493 (2018).

7. T.A. Taha, A.A. Azab, and M.A. Sebak, *J. Mol. Struct.* 1181, 14 (2019).
8. M. Tadic, D. Markovic, V. Spasojevic, V. Kusigerski, M. Remskar, J. Pirnat, and Z. Jaglici, *J. Alloys Compd.* 441, 291 (2007).
9. R.D. Zysler, D. Fiorani, and A.M. Testa, *J. Magn. Magn. Mater.* 224, 5 (2001).
10. R.D. Zysler, M.V. Mansilla, and D. Fiorani, *Eur. Phys. J. B* 41, 171 (2004).
11. S. El-Rabaie, T.A. Taha, and A.A. Higazy, *Mater. Sci. Semicond. Process.* 30, 631 (2015).
12. S. El-Rabaie, T.A. Taha, and A.A. Higazy, *Mater. Sci. Semicond. Process.* 34, 88 (2015).
13. S. El-Rabaie, T.A. Taha, and A.A. Higazy, *Appl. Nanosci.* 4, 219 (2014).
14. H. Donya and T.A. Taha, *J. Mater. Sci.: Mater. Electron.* 29, 8610 (2018).
15. S. El-Rabaie, T.A. Taha, and A.A. Higazy, *J. Alloy. Compd.* 594, 102 (2014).
16. V. Marghussian, *Nano-Glass Ceramics: Processing, Properties and Applications* (William Andrew, 2015).
17. S. Ram, *Phys. Rev. B* 51, 6280 (1995).
18. R. Iordanova, Y. Dimitriev, V. Dimitriev, S. Kassabov, and D. Klissurski, *J. Non-Cryst. Solids* 201, 141 (1996).
19. A. Kumar, S.B. Rai, and D.K. Rai, *Mater. Res. Bull.* 38, 333 (2003).
20. M. Abo-Naf, F.H. El Batal, and M.A. Azooz, *Mater. Chem. Phys.* 77, 846 (2002).
21. P. Pascuta and E. Culea, *Mater. Lett.* 62, 4127 (2008).
22. P. Pascuta, R. Lungu, and I. Ardelean, *J. Mater. Sci.: Mater. Electron.* 21, 548 (2010).
23. P. Pascuta, *J. Mater Sci.: Mater. Electron.* 21, 338 (2010).
24. T.A. Taha and A.S. Abouhaswa, *J. Mater Sci.: Mater. Electron.* 29, 8100 (2018).
25. C.M. Hurd, *Contemp. Phys.* 23, 469 (1982).
26. T. Komatsu and N. Soga, *J. Chem. Phys.* 72, 1781 (1980).
27. A. Saqlain, M.U. Shah, and S.H. Alam, *Mater. Sci. Eng.* 31, 1010 (2011).
28. T.G. Avancini, M.T. Souza, A.P.N. de Oliveira, S. Arcaro, and A.K. Alves, *Ceram. Int.* 45, 4360 (2019).
29. H.Y. He, *Int. J. Appl. Ceram.* 11, 626 (2014).
30. T.A. Taha and A.A. Azab, *J. Mol. Struct.* 1178, 39 (2019).
31. T.A. Taha and A.A. Azab, *J. Electron. Mater.* 45, 5170 (2016).
32. A. Ciżman, E. Rysiakiewicz-Pasek, M. Krupiński, M. Konon, T. Antropova, and M. Marszałek, *Phys. Chem. Chem. Phys.* 19, 23318 (2017).
33. T.A. Taha, S. Elrabaie, and M.T. Attia, *J. Electron. Mater.* 48, 6797 (2019).
34. J.C. Giuntini, J.V. Zanchetta, D. Jullien, R. Eholie, and P. Houenou, *J. Non-Cryst. Solids* 45, 57 (1981).